Evolution of the X-ray Luminosity in Young HII Galaxies*

D. Rosa González[1], E. Terlevich[1][†], E. Jiménez Bailón[2], R. Terlevich[1][†], P. Ranalli[3], A. Comastri[4], E. Laird[5] and K. Nandra[5]

[1] *Instituto Nacional de Astrofísica Optica y Electrónica. Luis Enrique Erro No. 1. Tonantzintla, Puebla, C.P. 72840, México*
[2] *Instituto de Astronomía, Universidad Nacional Autónoma de México, Apartado Postal 70-264, 04510-México DF, México*
[3] *Universitá di Bologna - Dipartimento di Astronomia - via Ranzani 1 - 40127 Bologna, Italy*
[4] *INAF - Osservatorio Astronomico di Bologna, via Ranzani 1, 40127 Bologna, Italy*
[5] *Astrophysics Group, Imperial College London, Blackett Laboratory, Prince Consort Road, London SW7 2AZ*

ABSTRACT

In an effort to understand the correlation between X-ray emission and present star formation rate (SFR), we obtained XMM-Newton data to estimate the X-ray luminosities of a sample of actively starforming HII galaxies. The obtained X-ray luminosities are compared to other well known tracers of star formation activity such as the far infrared and the ultraviolet luminosities. We also compare the obtained results with empirical laws from the literature and with recently published analysis applying synthesis models. We use the time delay between the formation of the stellar cluster and that of the first X-ray binaries, in order to put limits on the age of a given stellar burst. We conclude that the generation of soft X-rays, as well as the Hα or infrared luminosities is instantaneous. The relation between the observed radio and hard X-ray luminosities, on the other hand, points to the existence of a time delay between the formation of the stellar cluster and the explosion of the first massive stars and the consequent formation of supernova remnants and high mass X-ray binaries (HMXB) which originate the radio and hard X-ray fluxes respectively. When comparing hard X-rays with a star formation indicator that traces the first million years of evolution (e.g. Hα luminosities) we found a deficit in the expected X-ray luminosity. This deficit is not found when the X-ray luminosities are compared with infrared luminosities, a star formation tracer that represents an average over the last 10^8 years. The results support the hypothesis that hard X-rays are originated in X-ray binaries which, as supernova remnants, have a formation time delay of a few mega years after the starforming burst.

Key words: Galaxies: evolution – Galaxies: starburst – X-rays: galaxies

1 INTRODUCTION

X-ray emission in star forming galaxies is dominated by a combination of high mass X-ray binaries (HMXBs), hot O-stars, young supernova remnants and hot plasma, all sources that are closely related to the presence of massive short-lived stars which directly trace the current star formation activity (Persic & Rephaeli 2002). Based on observations of local galaxies and the comparison with other tracers of recent star formation activity, several authors have proposed the use of the X-ray luminosity as a star formation tracer [e.g. David, Jones, & Forman (1992), Grimm, Gilfanov &

Sunyaev (2003), Ranalli, Comastri & Setti (2003)]. The locally observed correlations appear to hold also at high-z and an empirical L_X-SFR relation based on observations of Lyman Break Galaxies (LBGs) in the 1 Ms CDF-N has been derived (Nandra et al. 2002). However studies of LBGs suffer from the lack of other direct SFR tracers (e.g. Hα, FIR), and additionally, LBGs whose emission is dominated by starburst events are too faint to be directly detected. Only the *mean* X-ray luminosities are attainable, making the possible contamination by obscured AGN difficult to quantify (Persic et al. 2004). Recent papers have confirmed the use of the X-ray emission as a direct tracer of star formation events [e.g. Laird et al. (2005), Rosa-González et al. (2007a)]; in contrast, Barger, Cowie & Wang (2007) found a poor correlation between the X-ray and radio emissions of starforming galaxies that could question the use of X-rays as a reliable tracer of star formation activity. In a recent paper

---

by Mas-Hesse, Otí-Floranes & Cerviño (2008), the different empirical relations between X-ray luminosities and the current SFRs were compared against evolutionary models. They found that under realistic assumptions (e.g. a young burst and an efficiency of a few percent in the re-processing of mechanical energy) the observed relations confirm the use of the soft X-ray luminosity as a reliable tracer of the star formation activity in young systems.

This paper discusses the X-ray emission (as detected by *XMM-Newton*) of HII galaxies selected from the Terlevich et al. (1991) catalog as having intense Hα and Hβ emission lines in their optical spectra.

HII galaxies are compact systems dominated by a strong and recent star formation burst event. The relative low mass – which implies a low contamination by low mass X-ray binaries – together with the absence of AGN activity make these objects the best laboratories to study the relation between the X-ray luminosity (L_X) and the current star formation rate (SFR). By using other tracers of star forming activity we will discuss the validity of the existing X-ray calibrations in very young systems. In fact, HII galaxies which are the youngest starbursts known in the local universe (Rosa-González et al. (2007b) could have a deficit of X-ray emission due to a time lag between the formation of the massive star cluster and the formation of the first HMXBs. In the following section we discuss the sample selection. In section 3, the data and its analysis. A comparison between the X-ray results and those obtained with other tracers of star formation is presented in Section 4. Section 5 is the discussion and conclusions are given in section 6.

Throughout this work a standard, flat ΛCDM cosmology with $\Omega_\Lambda = 0.7$ and $H_0 = 70$ km s^{-1} Mpc^{-1} is assumed.

2 SAMPLE SELECTION AND SFRS FROM OPTICAL EMISSION LINES

HII galaxies harbour intense and young star formation events revealed by the strong emission lines observed in the optical spectra. From the Spectrophotometric Catalog of HII galaxies (Terlevich et al. (1991) we have selected those galaxies for which the corresponding SFR is greater than 4 $M_\odot yr^{-1}$. Based on the calibration given by Grimm et al. (2003) and the estimated SFR, we expect to find at least 12 HMXBs with luminosities greater than 10^{38} erg s^{-1} in each one of the selected galaxies. Due to the galaxies low mass, the expected number of LMXBs is a minimum. The selected sample is given in Table 1.

The luminosities of the hydrogen recombination lines are proportional to the number of ionizing photons so they trace the presence of massive stars with lifetimes not larger than a few million years. We estimate the star formation rate from the reddening corrected Hα luminosities [SFR(Hα)] using the relation (Kennicutt 1998),

$$SFR(H\alpha)(M_\odot yr^{-1}) = 7.9 \times 10^{-42} L(H\alpha)(erg\, s^{-1}) \qquad (1)$$

Hα and Hβ fluxes are corrected for extinction using the Milky Way extinction curve (Seaton 1979) and assuming an intrinsic ratio Hα/Hβ of 2.87. The ionizing massive young clusters show in their spectra strong absorptions in the permitted lines (e.g. the HI Balmer series). The same species produces (at the same wavelengths) strong emission lines

in the ionized gas and therefore the observed intensity of such lines is reduced by the underlying absorption, affecting the derived extinction. For those galaxies for which the Hγ line flux was avaliable, we estimate the correction due to the presence of the low mass underlying population following Rosa-González, Terlevich & Terlevich (2002). The final values of Av (the extinction in the V wavelength given in magnitudes) together with the Hα and Hβ fluxes and the derived SFRs are presented in Table 1.

Notice that, as mentioned before, the SFR given by the Hα luminosity is tracing only the most massive stars (a few million years old), when a fraction of the expected HMXBs has yet to be formed. The time delay between the formation of the stellar burst and the formation of the first HMXBs, is one of the main topics of this paper and we will discuss it in detail in Section 4.

3 *XMM-Newton* DATA ANALYSIS

Fourteen objects have been observed with *XMM-Newton* (Jansen et al. 2001). The details of the observations are summarized in Table 2. The raw data have been processed using the standard *Science Analysis System*, SASv7.0.0 (Gabriel et al. 2004). The most up-to-date calibration files available in July 2007 have been used for the data reduction. The raw data have been filtered from high background flaring using the method described in Piconcelli et al. (2004). Detailed spatial and spectral analysis was possible only for four objects; net count rates were derived for all targets in the sample (Table 2). None of the objects was detected with the Reflection Grating Spectrometer.

3.1 Imaging Analysis

The majority of the sources are very weak in the X-ray band, allowing spatial analysis for only four of the galaxies: Mrk 52, Tol 1457, Tol 1247, and Cam 0902. We have generated smoothed images for these galaxies by applying the SAS task *asmooth*[‡] to the *pn* 0.2-2 keV, 2-12 keV and 0.2-12 keV band images (Figures 1, 2, 3, and 4).

The images of Mrk 52 in different energy bands (Fig. 1) show a soft source, with no significant emission in the hard band. This is also the case of Tol 1247-232 (Fig. 4), although its emission in the hard band is stronger that in Mrk 52. The images of Cam 0902+1448 in the different energy bands are shown in Fig. 2. Tol 1457-262 is actually an HII galaxy pair. Both components are detected in the X-ray image but could not be resolved (Fig 3). The images show that the South-West member is the weakest one of the pair, with a stronger contribution in the hard band, i.e. 2-12 keV.

3.2 Spectral analysis

For the majority of the sources (ten out of fourteen), the limited signal–to–noise did not allow spectral analysis with the EPIC camera. However, enough counts were detected to produce spectra for four sources: Mrk 52, Cam 0902, Tol 1457,

---

[‡] The *asmooth* task was applied using the *adaptive* convolution technique with a S/N=8.

Table 1. Optical emission lines: fluxes, visual extinctions and SFRs.

Name	Distance (Mpc)	F(Hα)(10^{-14}) (erg s^{-1}cm^{-2})	F(Hβ) (10^{-14}) (erg s^{-1}cm^{-2})	Av	SFR(Hα) $M_\odot$yr^{-1}
Mrk52	31	146. $\pm$ 22.	17.0$\pm$2.5	3.06$\pm$0.46	14.42$\pm$4.84
Cam0902+1448	222	28.1 $\pm$ 4.2	3.40$\pm$0.51	1.92$\pm$0.29	50.48$\pm$10.92
Tol1457-262	74	85.8 $\pm$ 13.	19.4$\pm$2.9	1.50$\pm$0.22	10.74$\pm$2.10
Tol1247-232	213	50.4 $\pm$ 7.6	13.5$\pm$2.02	0.74$\pm$0.11	36.52$\pm$12.25
Tol2259-398	127	19.9 $\pm$ 3.0	3.09$\pm$0.46	2.25$\pm$0.34	14.95$\pm$5.02
Cam08-82A	222	9.43 $\pm$ 1.4	1.10$\pm$0.16	3.05$\pm$0.46†	38.45$\pm$12.90
Mrk605	131	8.07 $\pm$ 1.2	1.00$\pm$0.15	2.87$\pm$0.43†	10.15$\pm$3.40
Tol2306-400	292	9.50 $\pm$ 1.4	0.87$\pm$0.13	3.71$\pm$0.56†	106.99$\pm$35.89
Mrk930	78	39.4 $\pm$ 5.9	8.91$\pm$1.34	1.20$\pm$0.18	5.34$\pm$1.79
UM530	316	26.9 $\pm$ 4.0	4.37$\pm$0.65	2.12$\pm$0.32	114.40$\pm$38.37
Tol0420-414	87	86.0 $\pm$ 13.	28.2$\pm$4.23	0.17$\pm$0.02†	6.93$\pm$2.32
Tol0619-392	236	9.53 $\pm$ 1.4	1.23$\pm$0.18	2.76$\pm$0.41	35.72$\pm$11.98
UM421	177	3.17 $\pm$ 0.48	0.24$\pm$0.04	4.24$\pm$0.64†	19.02$\pm$6.38
UM444	105	17.1 $\pm$ 2.6	3.24$\pm$0.49	1.20$\pm$0.18	4.15$\pm$1.39

Av corrected by an underlying stellar population except when marked with a †

Table 2. *XMM-Newton* observations ID, total and net exposure times after flaring removal, and background subtracted count rates in the different X-ray bands. The data were extracted from the *EPIC-pn* camera.

| Target	Obs. ID	Exposure time ks	Count Rate (0.15 - 10 keV) c/s	Count Rate (0.5 - 2 keV) c/s	Count Rate (2 - 10 keV) c/s
Mrk 52	0303560101	6.84, 4.3	0.020$\pm$0.002	0.0132$\pm$0.0018	0.0008$\pm$0.0003
Cam 0902+1448§	3035620101	6.84, 3.3	0.110$\pm$0.011	0.053$\pm$0.006	0.030$\pm$0.008
Tol 1457-262	0303560601	9.33, 6.5	0.059$\pm$0.004	0.040$\pm$0.003	0.013$\pm$0.003
Tol 1247-232	0303561001	11.5, 6.0	0.024$\pm$0.003	0.0150$\pm$0.0019	0.0058$\pm$0.0014
Tol 2259-398	0303560701	10.2, 5.6	0.010$\pm$0.003	0.0057$\pm$0.0019	0.004$\pm$0.003
Cam 08-82A	0303561101	11.8, 6.7	$<1.4\times10^{-3}$	$< 5 \times 10^{-4}$	$< 6 \times 10^{-4}$
Mrk 605	0303561701	7.93, 5.2	$(1.9\pm1.5)10^{-3}$	$< 9 \times 10^{-4}$	$< 9 \times 10^{-5}$
Tol 2306-400	0303560401	10.9, 5.0	$(8\pm3)10^{-3}$	$(4.9\pm1.6)10^{-3}$	0.003$\pm$0.002
Mrk 930	0303560901	10.8, 2.4	$(4.6\pm1.7)10^{-3}$	0.0017$\pm$0.0007	0.0029$\pm$0.0009
UM 530	0303560501	6.84, 2.0	$(8\pm3)10^{-3}$	$(5\pm2)10^{-3}$	$< 4 \times 10^{-4}$
Tol 0420-414	0303561901	6.84, 2.8	$(1.8\pm1.6)10^{-3}$	$(1.4\pm0.9)10^{-3}$	$< 3 \times 10^{-4}$
Tol 0619-392	0303561401	6.84, 3.5	$(5.2\pm2.3)10^{-3}$	$3.0\pm1.4)10^{-3}$	0.0020$\pm$0.0015
UM 421	0303561601	11.8, 5.7	$(2.9\pm1.7)10^{-3}$	0.0017$\pm$0.0011	0.0012$\pm$0.0009
UM 444	0303561801	12.1, 3.6	$(7\pm3)10^{-3}$	$(4.8\pm1.5)10^{-3}$	$< 8 \times 10^{-4}$

§ Another observation of Cam0902+1448 with ID 0303561201 is available. The results on spectral quantities derived from it, though less accurate, are compatible with those obtained from the 3035620101 observation so we used the latter for the analysis.

and Tol 1247. Circular extraction regions of 400, 700, 550 and 650 pixels respectively were selected in order to maximize signal–to–noise in the 0.2-10 keV band (see details in Piconcelli et al. (2004). By using these regions we are including between 80% and 90% of the total energy as described in the *XMM-Newton* handbook. We also checked that we are not including X-ray emission from close sources and from pixels too close to the CCD edges.

Background spectra have been extracted from a circular region located in the frame of the galaxy and free of any visible contaminating source. The associated ancillary and response matrices were obtained using the standard SAS tasks. *EPIC-pn* and the combined *MOS* 1 and 2 spectra of the four brightest objects were extracted. The spectra of Cam 0902+1448, Tol 1457-262, and Tol 1247-232 have been binned such that each bin contains at least 20 counts in order to apply the χ^2 minimization technique. As not enough counts were detected in Mrk 52, we used the unbinned spectra to perform the analysis and therefore C-statistics were

applied. The *XMM-Newton* spatial resolution and the limited signal–to–noise do not allow us to spectroscopically analyze each component of the pair Tol 1457 separately. Both members are included in the extraction region and therefore fluxes and luminosities refer to the pair's combined emission. In all the galaxies, the spectral analysis has been performed using the v12.0 of XSPEC. The errors quoted are referred to the 90% confidence level, i.e. $\Delta\chi = 2.71$ when χ^2 statistics were applied. In all the cases, we fixed the Galactic column density to the values listed in Table 5 which were obtained through the Leiden/Argentine/Bonn Survey of Galactic HI (Kalberla et al. 2005).

The high supernova rate occurring in star-forming regions produces an acceleration of the electrons to relativistic velocities. The scattering of these electrons with FIR photons, enhanced by the star-forming process results in non-thermal X-ray emission. This emission can, at first order, be modelled as a power law with an index in the range 1.6-1.8. However, observational studies on star-forming galaxies find
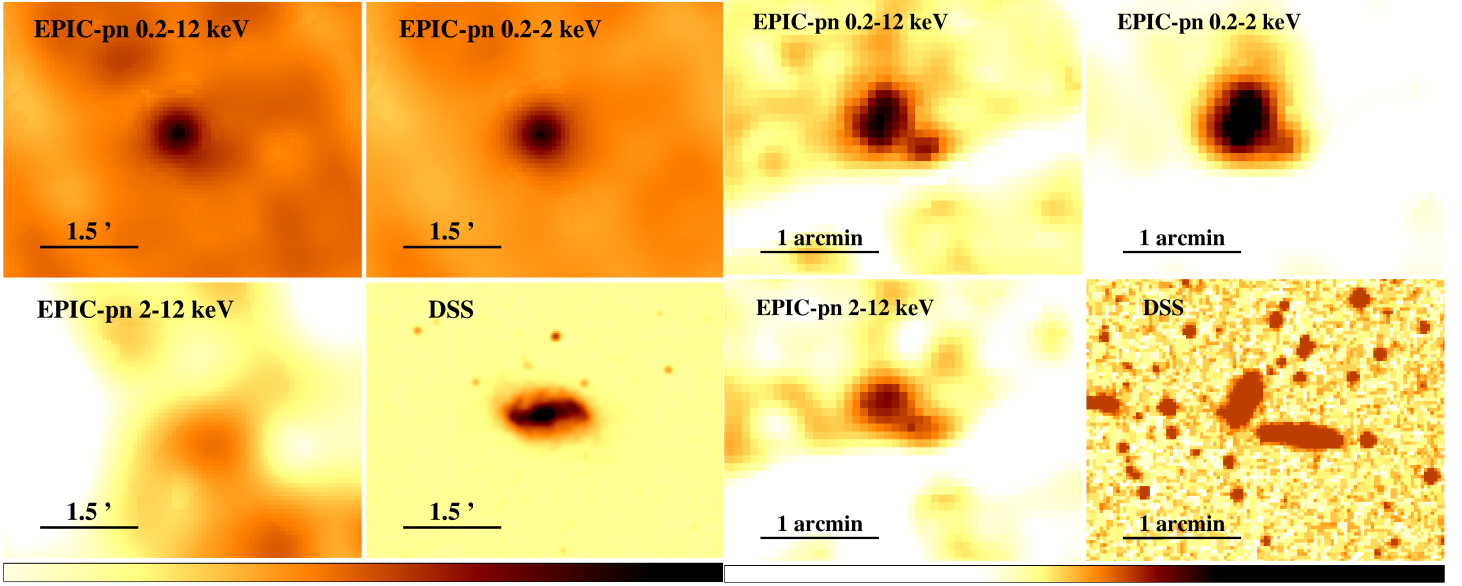
Figure 1. Smoothed *pn* images in the 0.2-12 keV, 0.2-2 keV, and 2-12 keV energy bands of Mrk 52. We also show the DSS image for comparison. Here and in figures 2, 3, and 4, North is up and East is left.
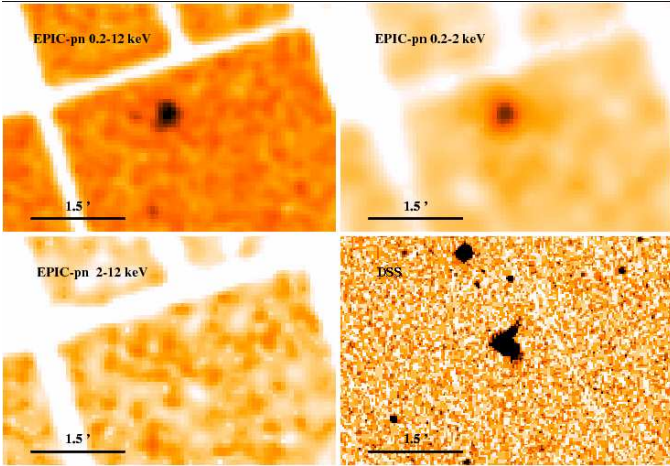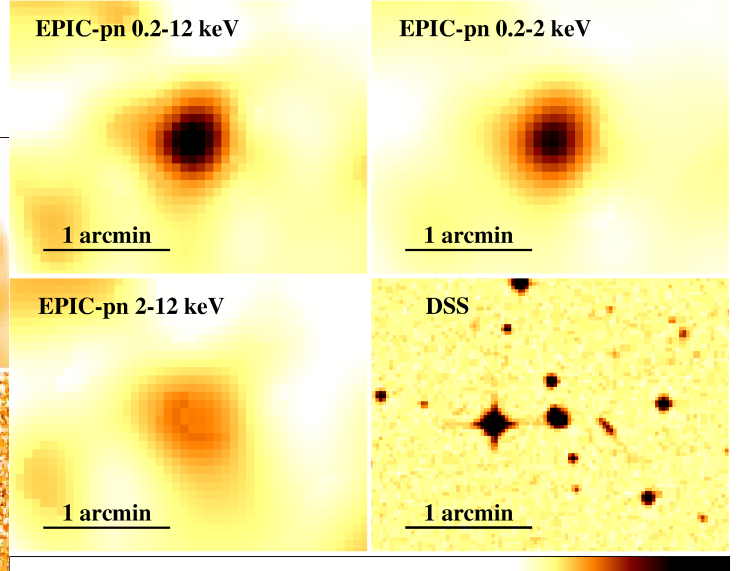

Figure 2. As in Figure 1, for Cam 0902+1448.

Figure 3. As in Figure 1, for Tol 1457-262.

Figure 4. As in Figure 1, for Tol 1247-232.

that a thermal emission model with temperatures of the order of 8 keV, provides also a satisfactory representation of the observed high energy spectra. The average X-ray spectrum of a population of low- and high-mass X-ray binaries can be described by a power law with an index $\Gamma \sim 1.2$ and a cut-off around 7.5 keV (Persic & Rephaeli 2003).

On the other hand, the diffuse emission mainly contributes to the soft X-ray band and can also be modelled as a thermal component but with a temperature one order of magnitude lower. Bearing this picture in mind, we have tested three different models to fit the source spec-

tra: a single power law, a thermal emission model [specifically the *mekal* model in XSPEC, Liedahl, Osterheld & Goldstein (1995)], and a combination of the best of the two previous ones with a second thermal emission model accounting for the soft emission. We also included a model for the photo electric absorption (*zwabs* in XSPEC) using the Wisconsin cross-sections (Morrison & McCammon 1983).

The parameters fitted – by using a Levenberg-Marquart method – and the goodness of the fits are given in Table 3. The low number of detected counts does not allow us to fit more complex models. A single-component model provides acceptable fits to the data for all sources analyzed, except for Cam 0902, for which a two components fit is best. The derived fluxes and unabsorbed luminosities for each object

are given in Table 4. In Figs 5 and 6, we illustrate the observed spectra and the best fit models for each galaxy. To illustrate the variation of the errors in the Γ vs. N_H and the temperature vs. N_H planes we plotted in Figure 7 the corresponding error ellipses for Cam 0902.

We compare the obtained X-ray fluxes (Table 4) with those given by a starburst model described below (Table 5). The agreement is good but some discrepancies were found in the soft X-ray fluxes mainly due to the uncertainties in the N_H value. In fact, differences in the goodness of the fit were found when the fit was made by fixing the value of the N_H derived from the Hydrogen emission lines ($N_H = 1.79 \times 10^{21} \times Av$, cm^{-2}) as compared with the results obtained when the N_H is a free parameter of the fitting procedure. The derived values of Γ are somewhat higher than those found in the literature for similar type of objects and fix $\Gamma = 2$ created fits with large values of χ^2. However the data quality does not allow the discussion of the origin of this apparent systematic effect. In one case (Cam 0902), the best fit was obtained by adding to the power law component a thermal model with a temperature of about 0.6 keV. That is consistent with temperatures of the hot plasma observed in other star forming galaxies (Grimes et al. 2005).

In order to have a homogeneous data set, and due to the low number of photons that could be affecting the conclusions obtained from the spectra, the analysis presented in the next sections is based only on the count rates from Table 2. The count rates were calculated for the *pn* detector, extracted from a region of 15″ free of contaminating sources and corrected for background. We convert the count rates by using a two component model; a power law with spectral index of 1.2 and a cut-off at 7.5 keV (associated to the combined high and low-mass X-ray binaries contribution) plus a thermal emission model with kT=0.8 keV (associated to the diffuse emission from galactic winds). The two components (power law and thermal emission) are normalized such that the flux ratio between the thermal and the power law components in the 2—10 keV band is 0.03 [(Persic & Rephaeli 2003), and references therein]. The estimated fluxes in the soft (0.5-2 keV) and hard (2-10 keV) bands are shown in Table 5. Calculations were performed using *PIMMS*v3.9[§].

The fluxes and luminosities, also given in Table 5, were corrected from absorption using the extinction derived from published ratios between Hα and Hβ which include the absorption due to the Galaxy. Notice that the values of the column density given in Table 5 were used only in the spectral analysis of Mrk52, Cam0902, Tol1457 and Tol1247. The errors were derived from the count rate uncertainties. However, we notice that they should be considered lower limits of the real uncertainties, as they only include the poisson error on the count rate. The uncertainty generated by considering different models is not included in the error budget. In this sense, when a single power-law model with $\Gamma = 2$ is applied instead of the cut-off power-law plus thermal emission, as suggested by other studies on single sources [e.g. NGC 3310, NGC 3690 by Zezas, Georgantopoulos, &

Ward (1998); NGC 253, M82 by Cappi et al. (1999)], differences of the order of 20 percent in the estimation of fluxes are obtained. The metallicity of the gas is another source of uncertainty particularly in the soft band. Calculations realized with *PIMMS* show that for a plasma with a temperature of 0.8 keV a change in metallicity from solar to 20% solar, typical of HII galaxies [e.g. Hoyos & Díaz (2006)], produces about 15% variation in the fluxes. Finally, we estimate the luminosity due to low mass X-ray binaries (L$_{LMXB}$) that could be present in the selected galaxies. Based on 2MASS K-band magnitudes we confirm that the observed galaxies have masses which are in general lower than that of an L$_\star$ galaxy (assuming a mass to light ratio in the K-band of 0.5, Bell & de Jong (2001). The contribution of these binaries to the observed X-ray luminosities is estimated using the relation between the stellar mass and the luminosity due to LMXB (Grimm, Gilfanov & Sunyaev (2002),

$$L_{LMXB}\,(erg\,s^{-1}) = 5 \times 10^{28} M_* \tag{2}$$

where M_* is the stellar mass in solar units. Table 5 shows that the calculated L_{LMXB} are much smaller, on average less than 2 percent and at most 20 percent, than the observed X-ray luminosities. The general result is that the total X-ray luminosities of the low mass galaxies selected here is probably not greatly affected by the LMXBs contribution.

4 EARLY EVOLUTIONARY PHASES: COMPARISON WITH SFR TRACERS

4.1 Hα luminosities

The recombination emission lines only appear during the early evolution of a starburst when the massive stars are hot enough to produce ionizing photons. Therefore, the deduced SFR(Hα) is tracing the first million years of the present starburst evolution. Figure 8 shows the relation between the Hα luminosity and the X-ray luminosities both in the soft (top panel) and in the hard (bottom panel) bands. The solid lines show the empirical relation found by Ranalli et al. (2003) based on the study of nearby star forming galaxies,

$$SFR_{soft}(M_\odot yr^{-1}) = 2.2 \times 10^{-40} L(0.5-2\,keV)\,(erg\,s^{-1}) \tag{3}$$

$$SFR_{hard}(M_\odot yr^{-1}) = 2. \times 10^{-40} L(2-10\,keV)\,(erg\,s^{-1}) \tag{4}$$

There is a good correlation between the L(Hα) and the soft X-ray luminosity (top panel), but there is one galaxy (Cam 0902+1448) for which the luminosity in X-rays is well above the one predicted by Ranalli's law. In the bottom plot of this Figure [hard X-rays vs. L(Hα)] most of the galaxies are below the empirical correlation. Due to the presence of upper limits we fit the luminosities by using survival analysis[¶]. The Buckley-James algorithm [BJ, e.g. Isobe, Feigelson, & Nelson (1986)] a non-parametric method which treats the residuals using the Kaplan-Meier description, was applied to the data in Figure 8. In the case of the bottom panel, the non-parametric method was applied both to all the data (dashed—line) and excluding Mrk52 (dotted—line).

[§] PIMMS does not consider the cut-off power-law for fluxes/count rates estimates. Therefore, we have also applied a correction due to differences on flux estimation when a simple power-law model is used instead of a cut-off power law.

[¶] See IRAF task stsdas.analysis.statistics.survival for an introduction to survival analysis.
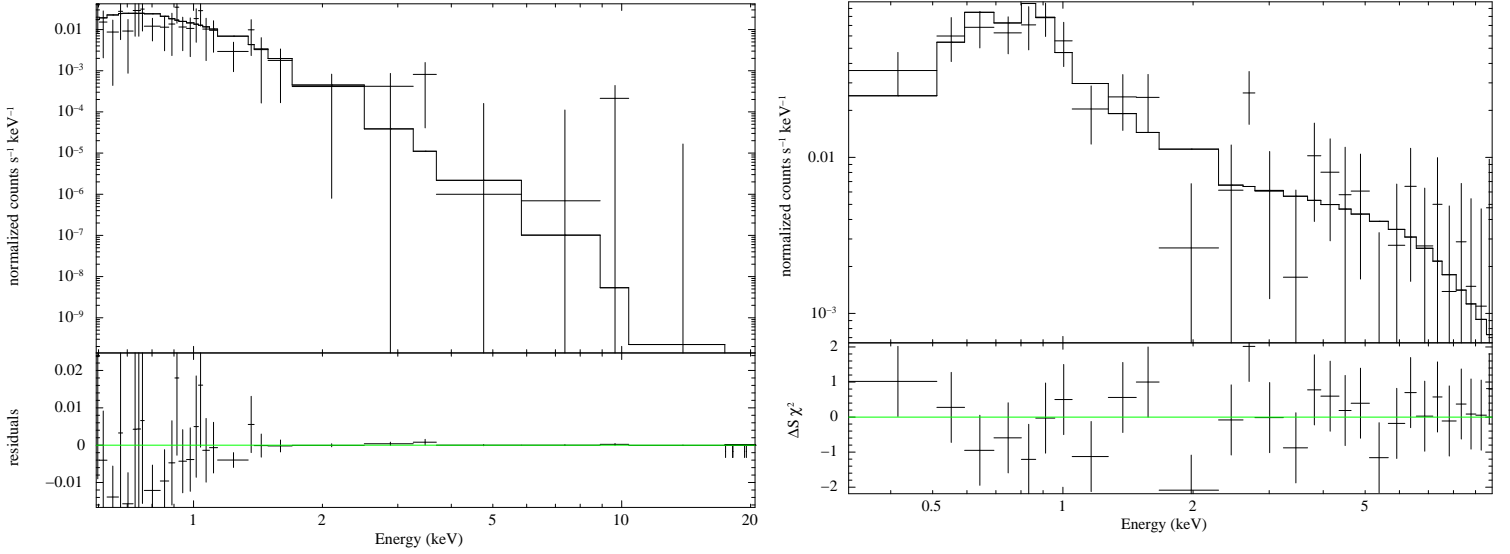
Figure 5. Observed *EPIC* spectra, best fit model and residuals of *left panel:* Mrk 52; *right panel:* Cam 0902+1448.
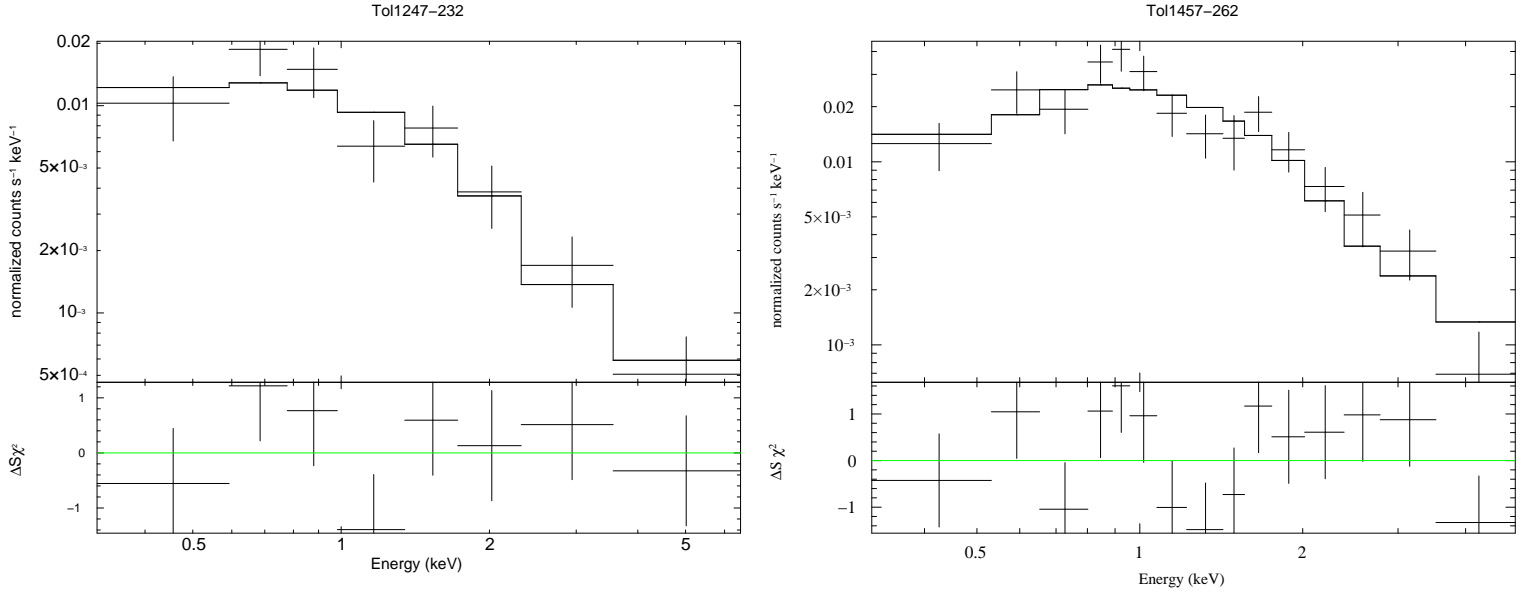
Figure 6. As in Figure 5 for *left panel:* Tol1247-232; *right panel:* Tol1457-262.

4.2   Radio luminosity

Table 6 shows the radio fluxes at 1.4 GHz for the selected galaxies extracted from NED. The strong correlation known to exist between the radio and the far infrared fluxes is taken as an indication that radio emission is a reliable tracer of the SFR. Yun, Reddy, & Condon (2001) found, from a FIR selected sample of about 1800 star-forming galaxies, that their radio continuum may be used to infer the extinction-free SFR using the relation

$$SFR(1.4\,GHz)(M_\odot yr^{-1}) = 5.9 \times 10^{-29} L(1.4\,GHz)(erg\,s^{-1}Hz^{-1}) \quad (6)$$

The values of SFR(1.4 GHz) for our *XMM-Newton* observed galaxies are also presented in Table 6. The empirical rela-

tion found by Yun et al. (2001) is well understood and it is based on the existence of a star forming event in which the observed radio emission arises from accelerated electrons produced in the supernova remnants and the IR radiation comes from dust that is heated mainly by massive stars. The estimated SFR corresponds to continuous star formation occurring for the last 10^8 years.

In Figure 9 we compare the radio with the soft X-ray luminosities together with the empirical relation given by Ranalli et al. (2003). In the left panel the X-ray luminosities are calculated by using a two component model (thermal + power law as described in section 3.2). Although the original calibration by Ranalli et al. (2003) is based on the relation between the radio and X-ray luminosities (solid line), a clear

Table 3. Spectral analysis.

Target	Model (1)	N_H $10^{21}\mathrm{cm}^{-2}$	Γ	N_H $10^{21}\mathrm{cm}^{-2}$	kT keV	Goodness
Mrk 52	**A**	6 ± 3	6.5 ± 0.5	-	-	**489 for 3222 dof‡**
	A†	5.5f	6.5 ± 0.5	-	-	490 for 3223 dof‡
	B	-	-	$7.7^{+1.5}_{-1.3}$	0.14 ± 0.02	497 for 3222 dof‡
	B†	-	-	5.5f	$0.18^{+0.02}_{-0.03}$	505 for 3223 dof‡
Cam 0902+1448	A	$4.6^{+1.8}_{-1.2}$	$5.2^{+0.8}_{-1.2}$	-	-	31 for 25 dof
	A†	3.4f	$5.3^{+0.3}_{-0.4}$	-	-	35 for 26 dof
	B	-	-	0.8	0.2	63 for 25 dof
	B†	-	-	3.4f	0.25	73 for 26 dof
	C	$2.0^{+1.5}_{-1.6}$	$3.6^{+1.2}_{-1.1}$	-	$0.63^{+0.16}_{-0.17}$	**18 for 23 dof**
Tol1457-262	**A**	$1.4^{+1.0}_{-0.9}$	$2.2^{+0.5}_{-0.4}$	-	-	**16.2 for 12 dof**
	B	-	-	< 0.6	$4.6^{+3}_{-1.5}$	18.7 for 12 dof
Tol1247-232	**A**	< 1.4	$1.8^{+0.4}_{-0.3}$	-	-	**5.1 for 6 dof**
	B	-	-	< 0.5	7^{+16}_{-4}	7.6 for 6 dof

Notes: (1) Model A: zwabs*zpowerlaw;Model B: zwabs*mekal; Model C: zwabs(zpowerlaw+mekal); in boldface, the best fit model.† N_H fixed to the value derived from A_V. ‡ C-statistics.

Table 4. Observed fluxes and unabsorbed luminosities in the soft and hard bands.

Target	Flux (0.5-2 keV) 10^{-14} erg cm $^{-2}$s^{-1}	Flux (2-10 keV) 10^{-14} erg cm $^{-2}$s^{-1}	Luminosity (0.5-2 keV) 10^{41} erg s^{-1}	Luminosity (2-10 keV) 10^{41} erg s^{-1}
Mrk 52	2.5 ± 0.5	0.08 ± 0.03	5.8 ± 1.2	$1.0 \pm 0.4 \times 10^{-3}$
Cam0902+1448	$8.5^{+1.5}_{-4}$	$1.5^{+0.4}_{-1.3}$	14^{+2}_{-7}	$1.1^{+0.3}_{-0.9}$
Tol1457-262	$5.5^{+1.3}_{-1.9}$	$8.5^{+1.5}_{-2}$	0.7 ± 0.2	$0.58^{+0.11}_{-0.14}$
Tol1247-232	$2.2^{+0.8}_{-1.3}$	$4.4^{+0.7}_{-2}$	$1.6^{+0.6}_{-0.9}$	$2.5^{+0.4}_{-1.1}$
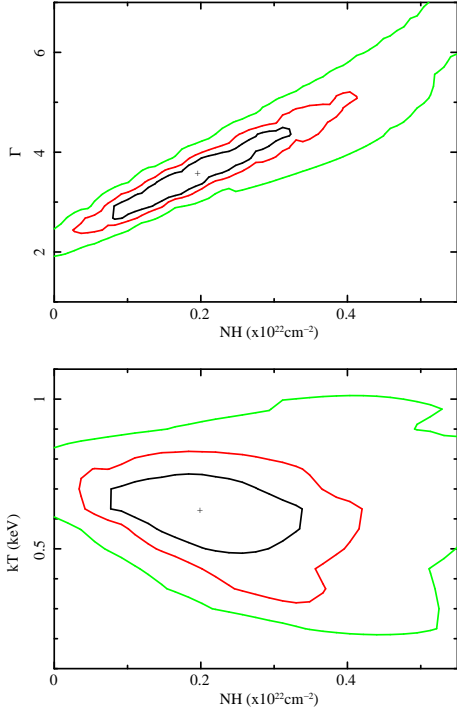
Figure 7. Confidence contours for the determination of Γ and N_H (top panel) and temperature and N_H (bottom panel) for Cam0902. In both panels the best fit is marked with a cross.
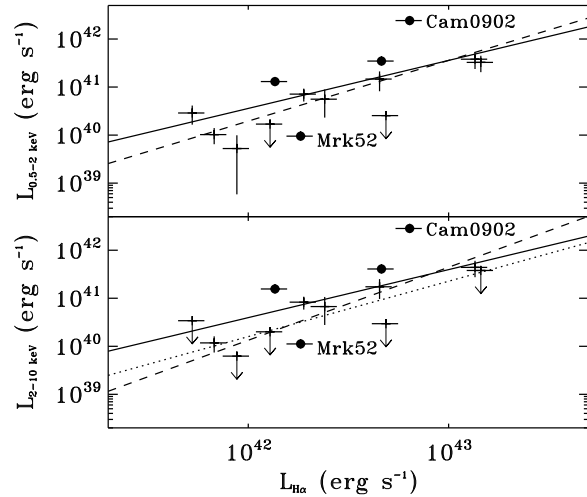
Figure 8. X-ray (soft band in the top and hard band in the bottom panel) vs. Hα luminosities. Here and in the following plots, solid circles mark those galaxies for which we extracted the X-ray spectrum. In both cases, the solid line is the result of converting the Ranalli law to Hα luminosities and the dashed one is a linear fitting that takes into account the presence of upper limits in the derived X-ray luminosities. In the bottom panel, the dotted line is the result of the fit obtained when leaving out the outlier Mrk52.

Table 5. Galactic column density and derived fluxes and luminosities.

Target	N_H (10^{20}) cm^{-2}	$F_{0.5-2\,keV}$ (10^{-14}) erg/s/cm	$F_{2-10\,keV}$ (10^{-14}) erg/s/cm	$L_{0.5-2\,keV}$ (10^{41}) erg/s	$L_{2-10\,keV}$ (10^{41}) erg/s	$L_{0.5-2\,keV}^{thermal}$ (10^{41}) erg/s	L_{LMXB} (10^{39}) erg/s
Mrk 52	1.9	8.40±0.88	9.90±1.04	0.10± 0.01	0.11± 0.01	0.048±0.005	1.76±0.53
Cam 0902+1448§	3.7	41.00±4.13	48.00±4.84	24.24± 2.44	28.38± 2.86	12.1 ±1.22	2.34±0.70
Tol 1457-262	9.4	20.00±1.36	24.00±1.63	1.30± 0.09	1.56± 0.11	0.651±0.044	0.47±0.14
Tol 1247-232	6.6	6.40±0.77	7.50±0.90	3.48± 0.42	4.07± 0.49	1.73±0.209	< 0.73
Tol 2259-398	1.1	3.70±1.11	4.30±1.29	0.71± 0.21	0.83± 0.25	0.357±0.107	1.04±0.31
Cam 08-82A	3.3	<0.43	<0.50	<0.25	< 0.30	< 0.127	< 0.63
Mrk 605	1.9	<0.82	<0.97	<0.17	< 0.20	< 0.085	1.36±0.41
Tol 2306-400	1.3	3.73±1.40	4.30±1.61	3.81± 1.43	4.39± 1.65	1.90 ±0.714	3.96±1.19
Mrk 930	5.5	1.40±0.52	1.61±0.60	0.10± 0.04	0.12± 0.04	0.051±0.019	< 0.08
UM 530	1.5	2.74±1.03	3.18±1.19	3.27±1.22	< 3.79	1.63 ±0.612	6.43±1.93
Tol 0420-414	2.5	0.58±0.52	0.69±0.61	0.05±0.05	< 0.06	0.026±0.023	< 0.13
Tol 0619-392	7.6	2.20±0.97	2.60±1.15	1.47± 0.65	1.73± 0.77	0.734±0.325	1.78±0.53
UM 421	4.1	1.50±0.88	1.80±1.06	0.56± 0.33	0.67± 0.39	0.280±0.164	2.28±0.69
UM 444	2.1	2.20±0.94	2.60±1.11	0.29±0.12	< 0.34	0.144±0.062	0.54±0.16

deviation from the empirical relation is obtained for our objects. Most of the galaxies are below the line defined by Ranalli and collaborators and seem to have low radio emission. These galaxies could be in an early stage previous to the synchrotron phase that appear with the first supernova explosions. At this phase the radio emission is dominated by free–free electrons produced in HII regions close to massive stars.

To check if a better correlation is found when only the X-ray thermal emission is considered we use a thermal model to convert the counts to luminosities. We used PIMMS and a thermal mekal kT=0.8 keV model with solar metallicity to derive the luminosities for all the galaxies in the sample. In this model we assume that we are counting photons produced by the interaction between the hot out-flowing wind and the ambient gas in the host galaxy (Grimes et al. 2005). In the right panel the X-ray luminosities correspond to the so defined thermal component only. In both panels the solid line represents the empirical relation of Ranalli and collaborators and the dashed line, the linear regression to our data.

The radio fluxes of five of the galaxies are just upper limits, so we implement the BJ algorithm to confirm the observed trends. The results are shown by the dot-dashed line in both panels of figure 9 and in figure 10.

4.3 IR and UV luminosities

As we mentioned before, the IR radiation is a good tracer of the SFR averaged over the last 10^8 years. However an unknown fraction of UV photons could have escaped the galaxy and consequently, the derived SFR would be underestimated. To solve this problem Heckman et al. (1998) and Buat et al. (1999) proposed to add the SFR calculated from the ultraviolet to that based on the IR. By adding the two contributions, on one hand one avoids the complex corrections that must be applied to the UV data and on the other hand, there is no need to correct for the uncertain UV escaping fraction that affects the IR measurements. We use the relations (Kennicutt 1998),

$$SFR(IR)(M_\odot yr^{-1}) = 4.5 \times 10^{-44} L(IR)(ergs^{-1}) \quad (6)$$

$$SFR(UV)(M_\odot yr^{-1}) = 1.4 \times 10^{-28} L_\nu(ergs^{-1}Hz^{-1}) \quad (7)$$

which are valid for the case of a universal Salpeter initial mass function with masses between 0.1 and 100 $M_\odot$. The UV data comes from GALEX (MAST Archive) and our UV observations made with OM on board *XMM-Newton* (Table 6). For those galaxies for which IRAS data exist, we estimate both the SFR(IR) and SFR(UV). The total SFR for them is calculated directly by adding the SFR(IR) and the SFR(UV) without applying any extinction correction. The results are given in Table 6. For those galaxies lacking IRAS data, the total SFR is calculated from the UV fluxes corrected by extinction, using Equation 7. To correct for extinction we use Calzetti's law (Calzetti 2001) and the visual extinctions calculated from the Balmer decrement (Table 1) but taking into account that due to gas surrounding the newly formed stars, they are more extinguished than the stars from which most of the UV radiation is coming [*age selective extinction*, e.g. Mayya et al. (2004)]. Cid Fernandes et al. (2005) based on the study of 50,362 galaxies from the Sloan Digital Sky Survey (SDSS) found that the relation between the visual extinction obtained from the Hα to Hβ ratio is $Av = 0.24 + 1.81Av^*$, where Av^* is the extinction that is affecting the continuum light. The Av^* values are the ones that we apply to correct the observed UV fluxes. The comparison of the total SFR with the X-ray luminosities is presented in Figure 11. The ratio between the soft X-ray and IR luminosities can be used to study the evolutionary stage of a given star forming burst. The values are given in Table 6 and a comparison with the results from recent theoretical models is discussed in the next section.

5 DISCUSSION

The strong hydrogen recombination lines observed in the selected galaxies suggest the presence of an intense burst younger than a few million years. In most of the cases, the derived SFR is higher than that of the archetypal starburst galaxy M82 (Mayya et al. (2004). In the early phases of the evolution of a star cluster (just before the first SN explosions) the soft X-rays are mainly produced by the me-
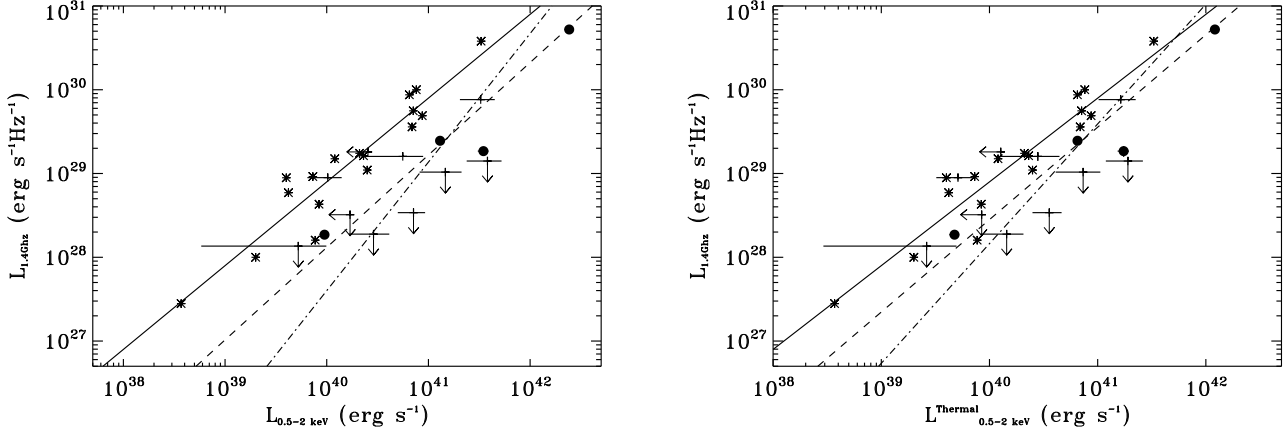
Figure 9. Radio versus soft X-ray luminosity ($L_{0.5-2kev}$) for the selected galaxies. The X-ray luminosities have been calculated by using a two model component (thermal + power law) in the left panel and a thermal component in the right panel. Galaxies for which it was possible to extract the spectra are marked with solid circles, the other sources in our sample are indicated as crosses. In both panels, the galaxies studied by Ranalli et al. are represented by asterisks. The solid line shows the linear correlation found by Ranalli and collaborators. The result of a standard linear fit (dashed line), and the fit from the survival analysis (dot—dashed line) are also plotted.

Table 6. Fluxes and SFRs from radio, infrared, ultraviolet and total. The ratio between the soft X-ray and IR luminosities is shown in the last column.

Name	F(1.4 GHz) (mJy)	SFR(1.4 GHz) $M_\odot \mathrm{yr}^{-1}$	F(60 μm) (Jy)	F(100 μm) (Jy)	SFR(IR) ($M_\odot \mathrm{yr}^{-1}$)	F(UV) (μJy)	SFR(UV) ($M_\odot \mathrm{yr}^{-1}$)	Tot. SFR ($M_\odot \mathrm{yr}^{-1}$)	$\log \frac{L_{0.5-2keV}}{L(IR)}$
Mrk52	13.10±0.60	1.10±0.33	4.43± 0.03	6.65± 0.10	1.47± 0.44	3086.38±36	0.61± 0.31	2.09± 1.2	-3.51
Cam0902+1448	86.84±0.82	309±93	4.12± 0.21	6.98± 0.35	62.1± 19.	1207.58±24	10.41± 5.2	72.6± 42	-2.76
Tol1457-262	37.80±1.80	14.5±4.4	3.09± 0.18	3.68± 0.41	4.34± 1.3	1670.91±21	1.52± 0.76	5.87± 3.4	-2.87
Tol1247-232	3.40±0.50	10.9±3.6	0.51± 0.05	< 0.97	10.6± 3.2	943.07±12	7.17± 3.6	17.8± 10.	-2.83
Tol2259-398	< 1.77	2.01	−	−	−	477.96±3.4	1.29± 0.64	10.1± 5.0	−
Cam08-82A	3.06±0.15	10.7±3.2	0.58± 0.01	0.95± 0.16	8.32± 2.5	203.48±3.9	1.68± 0.84	10.0± 5.8	−
Mrk605	< 1.56	1.90±4.3	0.27± 0.04	< 1.36	2.17± 0.65	172.18±4.3	0.50± 0.25	2.67± 1.6	−
Tol2306-400	< 1.38	8.31	<0.25	< 0.90	<9.86	325.57±11	4.65± 2.3	162± 81	−
Mrk930	12.20±0.90	5.26±1.6	1.25± 0.09	< 2.15	3.52± 1.1	864.69±18	0.88± 0.44	4.40± 2.6	-3.89
UM530	6.40±0.60	45.0±14	0.58± 0.07	0.63± 0.13	14.5± 4.3	340.44±17	5.68± 2.8	20.1± 12.	-2.99
Tol0420-414	< 1.50	0.80	<0.25	< 0.90	<0.87	160.44±5.6	0.20± 0.10	0.20± 0.1	−
Tol0619-392	< 1.56	6.14	0.42± 0.05	< 1.59	10.8± 3.2	238.70±7.8	2.23± 1.1	13.0± 7.6	-3.21
UM421	4.30±0.50	9.46±3.0	0.56± 0.07	< 1.30	8.07± 2.4	101.48±7.7	0.53± 0.26	8.60± 5.0	-3.51
UM444	< 1.44	1.11	<0.25	< 0.90	<1.27	465.66±7.8	0.85± 0.42	2.28± 1.1	−

chanical energy released by stellar winds [e.g. Strickland et al. (2002), Cerviño, Mas-Hesse, & Kunth (2002), Silich, Tenorio-Tagle, & Añorve-Zeferino (2005)], when the Hα luminosity is also stronger (Figure 8 top panel). The hard X-ray luminosity, on the other hand, is generally attributed to HMXBs (e.g. Grimm et al. (2003) which, at the early stages of evolution of these clusters are still in the formation process. In fact the maximum number of HMXBs occurs 20-50 Myr after the star forming event (Shtykovskiy & Gilfanov (2007). Therefore, a lack of hard X-rays is expected with respect to the *instantaneous* star formation rate traced by the Hα luminosity (Figure 8 bottom panel).

A dearth of radio emission in the early phases of cluster formation has been attributed either to a strong free–free absorption of the emitted radio waves (more severe at longer wavelengths), or to an epoch when most of the massive stars have not yet exploded as supernovae [Rosa-González at al. (2007b)]. Hα and hard X-ray luminosities probably differ because of the time delay between the formation of the

first SN remnants and the emergence of stellar winds in the cluster massive stars. Therefore it is hard to interpret SFRs based on different tracers which in general are related to different time scale phenomena. Figure 9 (radio vs. soft X-ray luminosities) shows the clear signature of a young starburst, where the radio luminosity is well below that expected from the Ranalli et al. (2003) relation. We have found that the SFR(1.4 GHz) is in general lower than the SFR(Hα) with the remarkable exception of Cam 0902+1448 for which the SFR(1.4 GHz) is about 6 times larger than the SFR(Hα). When we compare the radio luminosities with the soft X-ray luminosities and the Ranalli empirical relation the deficit in radio is noticeable (Figure 9). However, when we compare the radio luminosities with the fraction of the soft X-ray luminosities due to thermal emission alone, a better agreement is found (see right panel of Figure 9). Notice that when the BJ method is used to estimate the linear regression, a higher discrepancy is observed.

Radio versus hard X-ray luminosities are shown in Fig-

ure 10. We can see that most of the galaxies are below the relation proposed by Ranalli et al. (2003), consistent with the lack of both SN remnants and HMXBs.

For galaxies with avaliable IRAS data, the total SFR was calculated by adding the SFR(IR) and the SFR(UV) without correcting the UV fluxes for extinction. For those galaxies without IRAS fluxes, the total SFR was calculated from the extinction corrected UV luminosities. The total SFR is an average over the last 10^8 years, providing enough time for a population of HMXB to be in place. In fact there is a good correlation between the total SFR (averaged over the last 10^8 years) and the X-ray luminosities both in the soft and in the hard band (Figure 11), in fairly good agreement with the empirical Ranalli relation.

Notice that all selected galaxies are classified as HII galaxies based on BPT diagrams of optical line ratios. However an unknown contribution from a heavily obscured AGN could be present. This contribution is more important in the hard band, and the deviation from the Ranalli relation observed in Figure 10 could be due to an excess of X-ray emission from an AGN instead of representing a deficit in radio. However, such deficit in radio is clear when the SFR(Hα) is compared with the SFR(1.4 GHz). Moreover, the excess of hard X-ray emission is not present when comparing the hard band X-ray luminosity with the total SFR (Figure 11). We can safely conclude that the X-ray emission that we see is due to star formation processes.

Mas-Hesse et al. (2008) have concluded that assuming a reprocessing efficiency of the mechanical energy of a few percent, the observed values of the ratio between the soft X-ray and infrared luminosities can be reproduced with synthetic models of young starbursts. In fact they obtain an average value of $log\,L_{0.5-2keV}/L_{IR} = -3.5$ for efficiencies between 1% and 10% for bursts with ages around 5 Myr. In our sample, the ratio $log\,L_{0.5-2keV}/L_{IR}$ (Table 6) has an average value of -3.20 ± 0.41 consistent with the theoretical estimations. For continuous star formation, a value of $log\,L_{0.5-2keV}/L_{IR} = -3.5$ is consistent with ages as large as 25 Myr. At this age, a significant number of stars have exploded as SN. The strong emission lines and the high SFR derived together with the lack of synchrotron emission observed in most of the sources suggest a star formation history characterized by a strong short burst.

Mrk 52 and Cam0902 are outliers in some of the presented plots. Particularly, Mrk 52 is a bright blue galaxy with a derived SFR(Hα)=14 M$_\odot$yr^{-1}. However, the extremely weak emission in the hard X-ray band (see Figure 1) together with the deficit in radio makes this galaxy the most clear example of an extreme young burst with an age of about 3 Myrs when the majority of supernovae and HMXBs have not yet been formed. This age is consistent with Mrk 52 being a Wolf-Rayet galaxy as the dominant burst is going through an intense Wolf-Rayet phase [Schaerer, Contini, & Pindao (1999), Fernandes et al. (2004)].

6   CONCLUSIONS

We have analyzed *XMM-Newton* observations of a sample of 14 star forming galaxies with high SFR judging from their strong hydrogen recombination lines. The main conclusions of our analysis are:
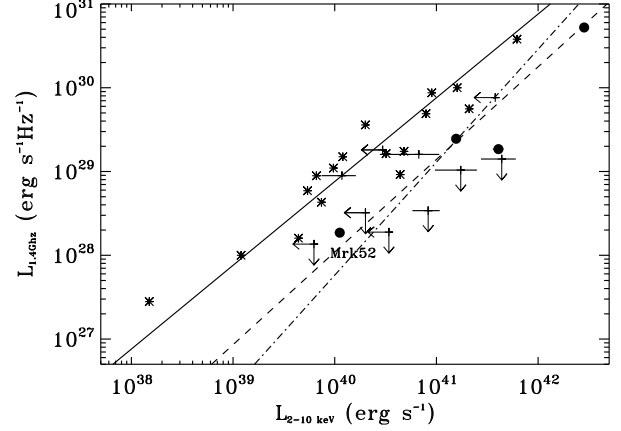
Figure 10. Radio vs. hard X-ray luminosities. Symbols as in Figure 9.
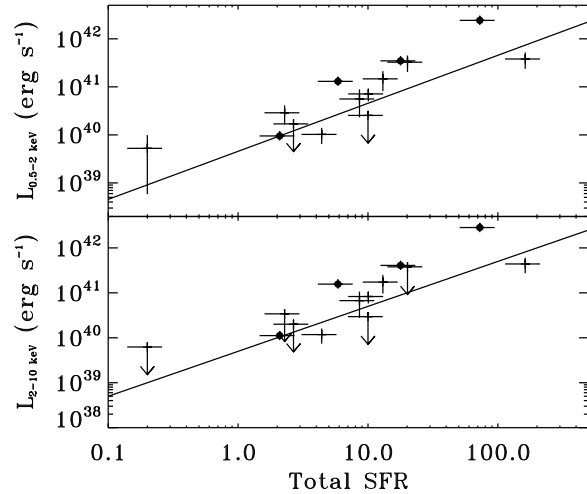
Figure 11. X-ray luminosity (top panel for the soft and bottom panel for the hard band) against the total SFR. The line shows the Ranalli empirical law for soft and hard X-ray luminosities. In both panels, solid circles are the bright X-ray objects in the sample with an X-ray spectrum.

(i) The SFR obtained from the soft X-ray luminosity is comparable to that determined from the Hα luminosities. This is consistent with the X-ray luminosity as a good tracer of SFR even at early times when the massive stars dominate the energy generation. Due to the time delay between the formation of the burst and the formation of the first massive binary systems, a lack of hard X-ray luminosity is observed when compared with tracers of recent star formation activity (e.g. Hα, Figure 8). This effect has already been observed in the Small Magellanic Cloud; we have extended the study to a larger sample of starforming galaxies.

(ii) The weak radio emission observed in some of the objects (related to early phases in the starburst evolution) together with the values found for $log\,L_{0.5-2keV}/L_{IR} \sim -3.2$ suggests that the sample of galaxies is biased to galaxies dominated by young bursts with ages lower than 5 Myrs and with star forming histories characterized by long and low activity periods, followed by strong short episodes.

(iii) The relation of both soft and hard X-ray luminosity

with the SFR traced by the IR and UV, shows that the X-ray production is maintained during at least 10^8 years.

REFERENCES

Barger A. J., Cowie L. L., Wang W.-H., 2007, ApJ, 654, 764
Bell E. F., de Jong R. S., 2001, ApJ, 550, 212
Buat V., Donas J., Milliard B., Xu C., 1999, A&A, 352, 371
Calzetti D., 2001, PASP, 113, 1449
Cappi M., Palumbo G. G. C., Pellegrini S., Persic M., 1999, AN, 320, 248
Cerviño M., Mas-Hesse J. M., Kunth D., 2002, A&A, 392, 19
Cid Fernandes R., Mateus A., Sodré L., Stasińska G., Gomes J. M., 2005, MNRAS, 358, 363
David L. P., Jones C., Forman W., 1992, ApJ, 388, 82
Fernandes I. F., de Carvalho R., Contini T., Gal R. R., 2004, MNRAS, 355, 728
Gabriel C., et al., 2004, ASPC, 314, 759
Grimes J. P., Heckman T., Strickland D., Ptak A., 2005, ApJ, 628, 187
Grimm H.-J., Gilfanov M., Sunyaev R., 2002, A&A, 391, 923
Grimm H.-J., Gilfanov M., Sunyaev R., 2003, MNRAS, 339, 793
Heckman T. M., Robert C., Leitherer C., Garnett D. R., van der Rydt F., 1998, ApJ, 503, 646
Hoyos C., Díaz A. I., 2006, MNRAS, 365, 454
Isobe T., Feigelson E. D., Nelson P. I., 1986, ApJ, 306, 490
Jansen F., et al., 2001, A&A, 365, L1
Kalberla P. M. W., Burton W. B., Hartmann D., Arnal E. M., Bajaja E., Morras R., Pöppel W. G. L., 2005, A&A, 440, 775
Kennicutt R. C., Jr., 1998, ARA&A, 36, 189
Laird E. S., Nandra K., Adelberger K. L., Steidel C. C., Reddy N. A., 2005, MNRAS, 359, 47
Liedahl D. A., Osterheld A. L., Goldstein W. H., 1995, ApJ, 438, L115
Mas-Hesse J. M., Otí-Floranes H., Cerviño M., 2008, A&A, 483, 71
Mayya Y. D., Bressan A., Rodríguez M., Valdes J. R., Chavez M., 2004, ApJ, 600, 188
Morrison R., McCammon D., 1983, ApJ, 270, 119
Nandra K., Mushotzky R. F., Arnaud K., Steidel C. C., Adelberger K. L., Gardner J. P., Teplitz H. I., Windhorst R. A., 2002, ApJ, 576, 625
Persic M., Rephaeli Y., 2002, A&A, 382, 843
Persic M., Rephaeli Y., 2003, A&A, 399, 9
Persic M., Rephaeli Y., Braito V., Cappi M., Della Ceca R., Franceschini A., Gruber D. E., 2004, A&A, 419, 849
Piconcelli E., Jimenez-Bailón E., Guainazzi M., Schartel N., Rodríguez-Pascual P. M., Santos-Lleó M., 2004, MNRAS, 351, 161
Ranalli P., Comastri A., Setti G., 2003, A&A, 399, 39
Rosa-González D., Terlevich E., Terlevich R., 2002, MNRAS, 332, 283
Rosa-González D., Burgarella D., Nandra K., Kunth D., Terlevich E., Terlevich R., 2007a, MNRAS, 379, 357
Rosa-González D., Schmitt H. R., Terlevich E., Terlevich R., 2007b, ApJ, 654, 226
Schaerer D., Contini T., Pindao M., 1999, A&AS, 136, 35
Seaton M. J., 1979, MNRAS, 187, 73P
Shtykovskiy P. E., Gilfanov M. R., 2007, AstL, 33, 437
Silich S., Tenorio-Tagle G., Añorve-Zeferino G. A., 2005, ApJ, 635, 1116
Strickland D. K., Heckman T. M., Weaver K. A., Hoopes C. G., Dahlem M., 2002, ApJ, 568, 689
Terlevich R., Melnick J., Masegosa J., Moles M., Copetti M. V. F., 1991, A&AS, 91, 285
Yun M. S., Reddy N. A., Condon J. J., 2001, ApJ, 554, 803
Zezas A. L., Georgantopoulos I., Ward M. J., 1998, MNRAS, 301, 915